Laser-Ablated Vortex Fluidic-Mediated Synthesis of Superparamagnetic Magnetite Nanoparticles in Water Under Flow

Xuan Luo,[†,‡] Ahmed H. M. Al-Antaki,[†] Thaar M. D. Alharbi,[†] Wayne D. Hutchison,[§] Yi-chao Zou,[∥] Jin Zou,[∥] Antony Sheehan,[⊥] Wei Zhang,*[‡] and Colin L. Raston*[†]

[†]Flinders Institute for NanoScale Science and Technology, College of Science and Engineering, and [‡]Centre for Marine Bioproducts Development, College of Medicine and Public Health, Flinders University, Adelaide, South Australia 5042, Australia

[§]School of PEMS, University of New South Wales, ADFA campus, Canberra BC, Australian Capital Territory 2610, Australia

[∥]Materials Engineering and Centre for Microscopy and Microanalysis, The University of Queensland, Brisbane, Queensland 4072, Australia

[⊥]TGR Biosciences Pty Ltd, 31 Dalgleish Street, Thebarton, Adelaide, South Australia 5031, Australia

S Supporting Information

ABSTRACT: Selective formation of only one iron oxide phase is a major challenge in conventional laser ablation process, as is scaling up the process. Herein, superparamagnetic single-phase magnetite nanoparticles of hexagonal and spheroidal-shape, with an average size of ca. 15 nm, are generated by laser ablation of bulk iron metal at 1064 nm in a vortex fluidic device (VFD). This is a one-step continuous flow process, in air at ambient pressure, with in situ uptake of the nanoparticles in the dynamic thin film of water in the VFD. The process minimizes the generation of waste by avoiding the need for any chemicals or surfactants and avoids time-consuming purification steps in reducing any negative impact of the processing on the environment.
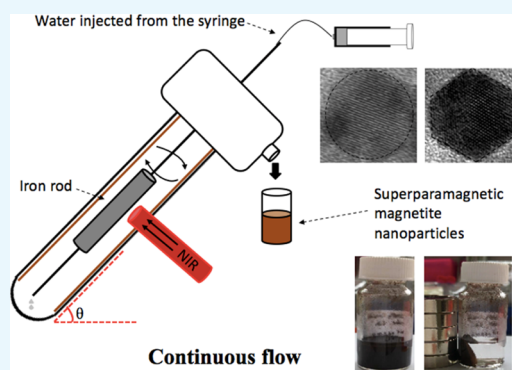
INTRODUCTION

The synthesis and availability of iron oxide nanoparticles (IONPs) are of general interest in many fields of research and in a number of applications. Some common phases of IONPs include α-Fe_2O_3 (hematite), Fe_3O_4 (magnetite), γ-Fe_2O_3 (maghemite), α-Fe (ferrite), Fe_3C (iron carbide), and FeO (wustite). For magnetite, IONPs smaller than 20 nm have superparamagnetic properties and are known as superparamagnetic IONPs.[1,2] This property relates to the large magnetic moment resulting from the coupling of the atomic spins within the nanosized magnetite nanoparticles.[3] Magnetite is one of the most intensively studied IONPs, which can be prepared using a number of different methods, including coprecipitation,[1] sol−gel,[4] microemulsion,[5] ultrasonic spray pyrolysis,[6] and microwave plasma.[7] They have different advantages and disadvantages relating to shape/size control, stability, scalability, monodispersity, and production cost. Among them, the coprecipitation method is relatively simple and fast and has potential for scaling up; however, it generates nanoparticles with a wide particle size distribution[1] and can generate a waste stream incorporating toxic chemicals.[8]

Pulsed laser ablation, which can be a simple and surfactant and counter-ion-free technique,[9] has been used to prepare magnetic nanoparticles with a narrow size distribution.[2] IONPs can be generated by laser ablation of bulk iron in either the gas or liquid phase,[10] the latter being the most studied,[11] with

Nd:YAG laser processing at 1064 nm affording nanoparticles with enhanced magnetic properties.[2] Water is the preferred solvent in terms of applications and environmental considerations, with the use of organic solvents generating amorphous carbon and iron carbide from its breakdown.[8,11,12] However, selectively forming only one iron oxide phase in water is a major challenge in laser processing.[2,9,12] Also, noteworthy is that after each laser pulse, the time taken for collapse of the plume is crucial in controlling the nucleation and growth of the IONPs;[2] longer times equate to longer growth times, affording mainly larger particles during the ablation in the liquid. On the other hand, laser ablation of an iron target in the gas phase can circumvent some of the above drawbacks for liquid ablation processing, using air as the oxidant.[13] Also, noteworthy is that the generation of nanoparticles from ablation in the gas phase is preferred because of increased yield relative to ablation in the liquid phase.[13] Maghemite has been generated by laser ablation in a mixture of nitrogen and oxygen under atmospheric pressure,[12] albeit with a broad size distribution of the particles, 5 to 90 nm in diameter. Laser ablation processing in the gas phase requires a more sophisticated setup with a specially designed ablation
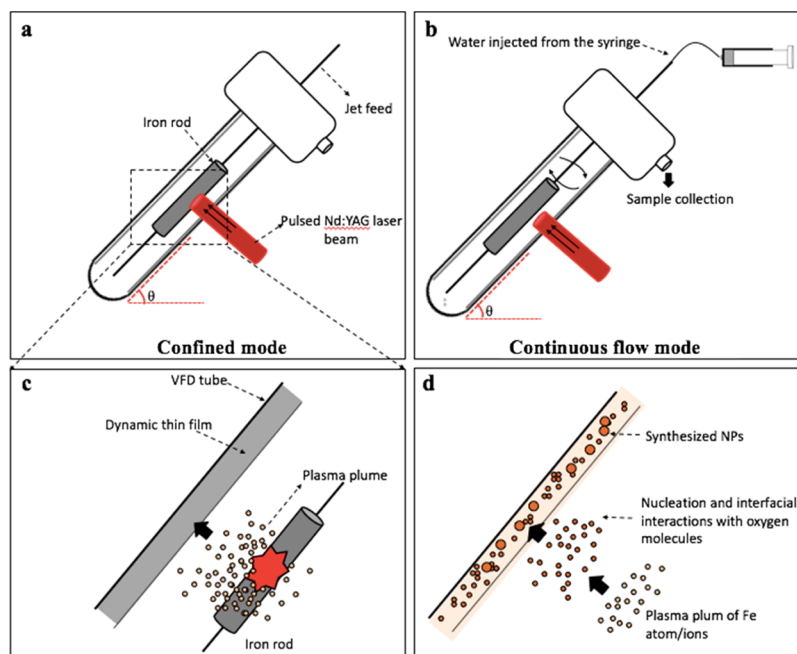
Figure 1. (a) Laser beam irradiation of an iron rod placed inside the VFD tube with the device operated in the confined mode. (b) Laser beam irradiation of an iron rod placed inside the VFD tube with the device operated in continuous flow mode. (c) Cartoon of a plasma plume containing iron atoms and ions. (d) Generating IONP through diffusion-driven nucleation and aggregation in the presence of a gas and a liquid carrier.

chamber and particle collector relative to liquid phase ablation.[13,14]

We were motivated to integrate laser ablation in both gas- and liquid-phases using the versatile vortex fluidic device (VFD) in association with an Nd:YAG pulsed laser, in developing a scalable process for preparing magnetite in water with control over the size of particles, and without requiring chemical additives. The VFD is a thin film microfluidic platform that is effective in high yield and controllable organic and material synthesis, in harnessing the intense micromixing, and high heat and mass transfer in the dynamic film.[15] Nd:YAG pulsed laser-assisted VFD processing has been used for fabricating graphene oxide scrolls from graphene oxides[16] and lateral slicing of high tensile strength carbon nanotubes[17] noting that in the absence of the laser, the mechano-energy in the film is effective in forming compact single-walled carbon nanotube toroids or rings.[18] The VFD is also effective in enhancing chemical reactivity and selectivity,[19] intensifying multiphase separation,[20] enhancing enzymatic reactions,[21] and in many more applications.[22] In the present study, the VFD was operated at 45° tilt angle for the rapidly rotating borosilicate glass tube (O.D. 20 mm, I.D. 17.5 mm), which is the optimal angle for a number of processes.[17−22] VFD processing can be conducted on small sub-milliliter scales in the so-called confined mode, where there is tilt-angle-dependent shear stress, as well as being upscaled under continuous flow, as shown in Figure 1. Polyvinyl pyrrolidine-coated superparamagnetic magnetite nanoparticles with a mean diameter of <10 nm have been previously fabricated using a coprecipitation method under continuous flow using a VFD with a 10 mm O.D. glass tube in an ammonia/nitrogen atmosphere.[23] Herein, we have established that the VFD with a 20 mm O.D. glass tube with higher volume capacity and safer laser ablation distance is effective in forming superparamagnetic magnetite nanoparticles with a narrow size distribution, as a one-step continuous flow process at ambient pressure. The

process is devoid of any gas flow which simplifies the setup and minimizes the generation of waste while avoiding the need for any chemicals/surfactants, as well as time-consuming purification steps in reducing any negative impact of processing on the environment.

RESULTS AND DISCUSSION

All of the optimization experiments were initially conducted with the VFD operated in the confined mode with 1 mL of water. The laser power was optimized first by conducting the experiment for 15 min at different laser powers, 20, 70, 160, 360, and 560 mJ, as shown in Figure 2a. Brown suspensions, as an indicator of the formation of iron oxide particles, were only obtained for experiments conducted at high laser power, at 360 and 560 mJ. The suspensions have a good colloidal stability for days, as shown in Figure 2b, in agreement with the zeta potential about +30 mV, as shown in Figure 2e. Post-VFD processing, the pH of the as-processed IONPs became slightly acidic relative to the Milli-Q water, affording positively charged particles.[24] As-prepared IONPs are not coated and are likely to agglomerate in water (Figure 2d) in reducing their large surface area to volume ratio, as reported by Demirer et al.[1] Iron-based nanoparticles lack sharp UV−vis spectrum absorption bands[8] but can be characterized by an absorption threshold for wavelengths lower than 400 nm (Figure 2c), typically representing different iron oxide phases of hematite, magnetite, and iron carbide.[8,25] The concentration of the as-prepared samples could be indirectly estimated using UV−vis spectroscopy with high absorbance associated with higher yield, as established by Fazio et al.[25] Figure 2c indicated that processing at 360 and 560 mJ generated the highest quantities of IONPs compared to other conditions. However, the borosilicate glass-tube VFD deteriorated with the risk of fracture using a laser power of 560 mJ, and accordingly the lower power of 360 mJ was used.
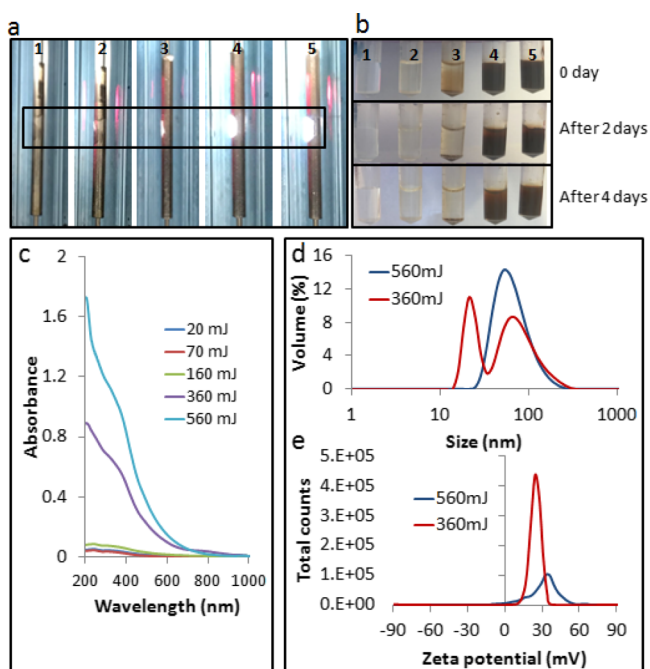
Figure 2. (a) Images showing the laser irradiation position with the iron rod placed inside the VFD tube spun at 7500 rpm with the 1064 nm pulsed laser operating at 20, 70, 160, 360, and 560 mJ, from samples 1 to 5, respectively. (b) As-prepared sample dispersed in 1 mL of water; a stable colloidal suspension was obtained for 360 and 560 mJ. (c) UV−vis spectra. (d) Dynamic light scattering results. (e) Zeta potential data.

Atomic force microscopy (AFM), transmission electron microscopy (TEM), and XRD analyses were carried out on the

samples ablated at 360 mJ, in establishing their composition and morphology. AFM revealed large aggregates of small spherical nanoparticles, as shown in Figure 3a, in accordance with TEM images that gave an estimated average particle of 12 nm, with a relatively narrow size distribution. XRD established that the material is either magnetite (COD 1011032) or maghemite (COD 9006316), with a crystallite size of ca. 14.2 nm, using the Debye−Scherrer equation, as shown in Figure 3b. The variation of the size estimation by XRD from TEM could be because of the presence of strain in the crystals that can lead to overestimation of particle diameters.[26] Raman spectroscopy can be used to differentiate between magnetite and maghemite.[27] The magnetite crystal belongs to the cubic space group $Fd3m$, having five Raman-active bands, A_{1g}, E_g, and three T_{2g}, and four infrared active bands T_{1u}.[28] The most intense band for magnetite (A_{1g} mode) was observed at 662 cm^{-1} (Figure 3b). Three smaller bands were observed at 192 (T_{2g}), 313 (E_g), and 526 (T_{2g}) cm^{-1} representing the phonon frequencies of magnetite. Two weak peaks between 1380 and 1600 cm^{-1} possibly correspond to graphitic material.[28] The yellow color of the solution after the migration of samples to a magnet (Figure 3a) can be ascribed to the presence of residual nanomagnetic amorphous carbon in solution, as described by Amendola et al.[8] Second-order Raman spectra are effective for determining the crystallinity of the carbon,[29] but the absence of such in this case (Figures S1 and S2) does not rule out the presence of amorphous carbon[30] that could arise from traces of storage solvent from the iron rod and fixation of carbon dioxide in the air. FTIR spectroscopy gave a band at 550 cm^{-1} corresponding to magnetite (Figure 3c), whereas maghemite has an analogous band at 600 cm^{-1}.[28,31] The black color of the samples is also consistent with magnetite being the dominant phase.[32]
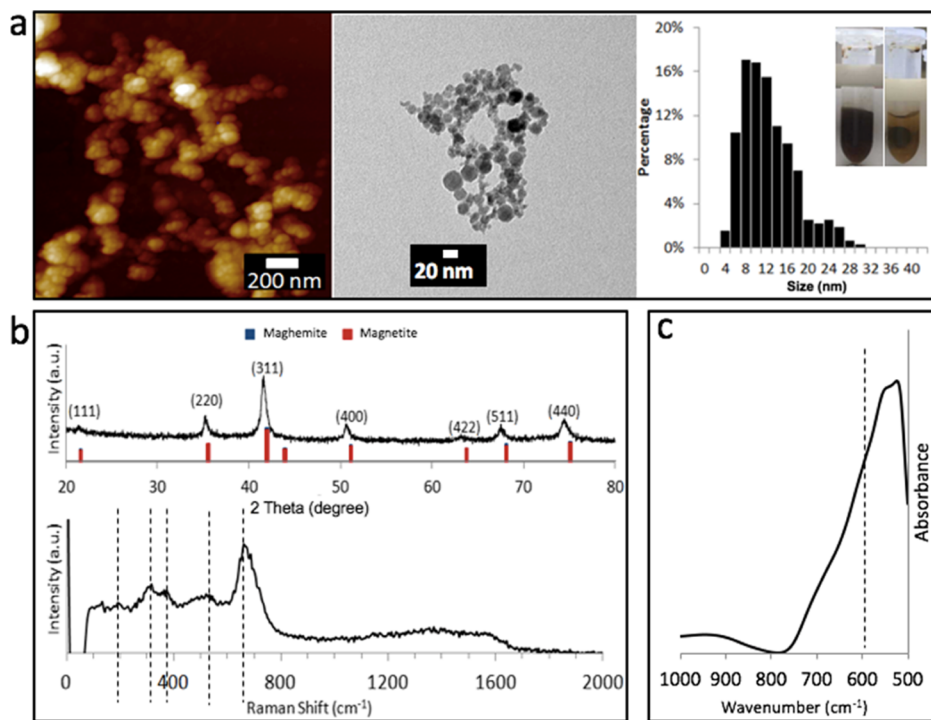

Figure 3. Characterization of the as-prepared IONPs (laser power 360 mJ for the VFD tube rotated at 7500 rpm for 15 min in the confined mode for 1 mL of water). (a) AFM, TEM, and size distribution plot which represented more than 300 randomly chosen IONPs. (b) XRD diffraction pattern and Raman spectra. (c) FT-IR spectrum.
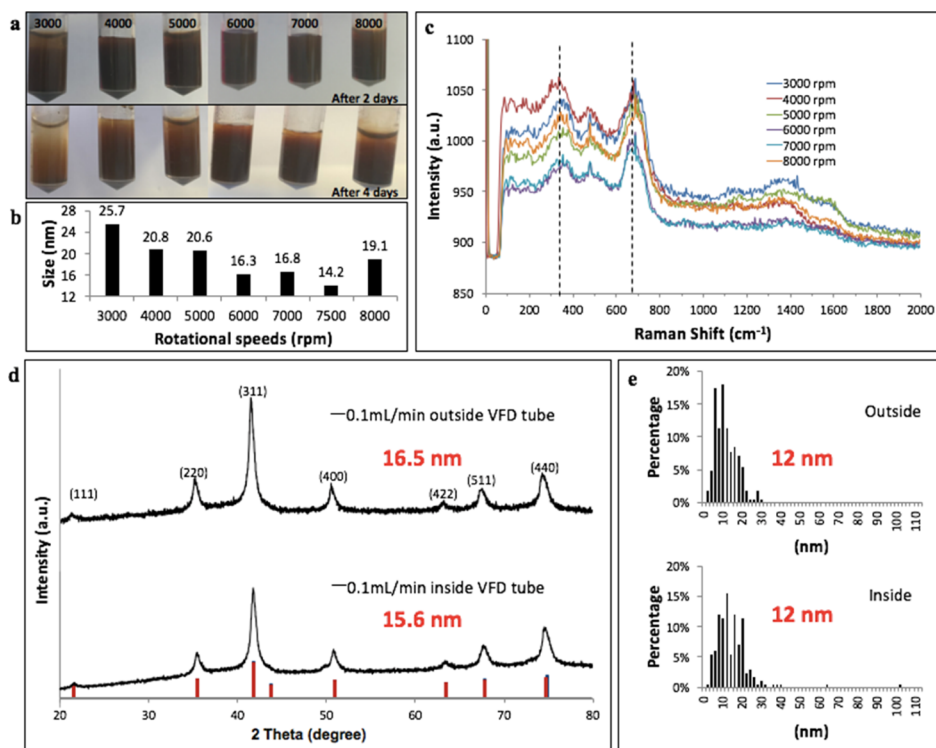
Figure 4. (a) Size of IONP nanoparticles generated at 360 mJ with the VFD operating in the confined mode containing 1 mL of water, for 15 min at different rotational speeds. (b) Particle size estimated using XRD. (c) Raman spectra. (d) XRD of samples conducted under continuous flow mode at 7500 rpm, 0.1 mL/min flow rate (materials exiting and retained inside the tube). (e) Size estimation plot based on TEM for two samples obtained from continuous flow (materials exiting and retained inside the tube).
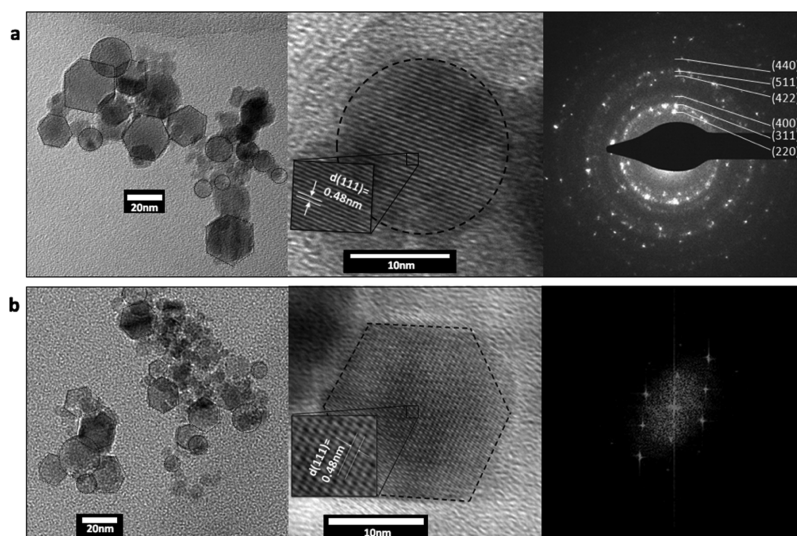

Figure 5. Representative TEM, HRTEM, and SAED (marked indices are planes of magnetite). (a) IONPs exiting the VFD operated at a rotational speed of 7500 rpm and a flow rate of 0.1 mL/min. (b) IONPs retained inside the tube during processing at a rotational speed of 7500 rpm and a flow rate of 0.1 mL/min. Both samples showed mixed shapes of spheres and hexagonal prisms. Both samples are single crystals with individual crystallites highlighted. The fast Fourier transform patterns were acquired from the HRTEM image.

Rotational speed of the VFD tube controls the size of the nanoparticle (Figure 4a,b), with the smallest size obtained at 7500 rpm, 360 mJ laser power, for 15 min in the confined mode, for 1 mL of water in the tube. The particles were rapidly formed during the laser ablation process with the shear presumably preventing the growth and coalescence of nanoparticles. XRD of these samples indicates the presence of magnetite or maghemite for all rotational speeds (Figure

S3). The weak Raman peak contribution at 720 cm^{-1} might arise from a small quantity of maghemite[28] at some rotational speeds (Figure 4c). Raman spectra were recorded using a significantly low laser power to avoid the transition of magnetite to maghemite or hematite as a result of local radiation.[24,33] A well-defined Fourier transform infrared (FT-IR) band at 550 cm^{-1} corresponding to magnetite was observed for all of these samples (Figure S4). To scale up the
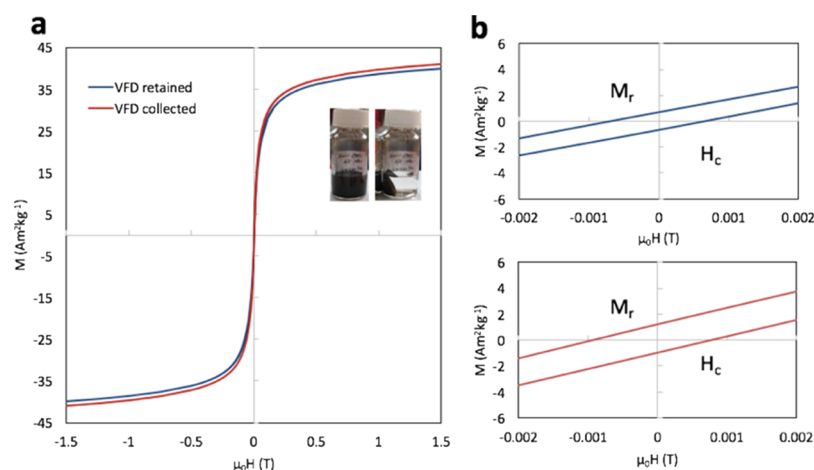
Figure 6. (a) Comparison of magnetic hysteresis curves of the VFD-processed samples (retained and collected). (b) Low-field interval of the magnetization curves of the two samples.

process, a continuous flow mode was used in which a syringe pump delivered water to the base of the VFD tube through a stainless steel jet feed. Flow rates were varied at 0.1, 0.5, and 1 mL/min, and the average size of particles derived from XRD data was 15.4 ± 1.1, 19.6 ± 1.0, and 20.3 ± 0.2 nm, respectively (Figure S5). A flow rate of 0.1 mL/min gave similar results (15.4 ± 1.1 nm) comparable to results for the confined mode, for 15 min processing time (14.2 nm). Thus, the processing time in the VFD is critical for controlling the nucleation and growth of the particles. In continuous flow mode, the solution-laden IONPs whirl up the rotating tube, exiting through a Teflon housing unit. This ensures more uniform processing during the laser irradiation, affording a more monodispersed size distribution.[11] Post-processing at 0.1 mL/min, deep brown fine particles were distributed along the VFD tube (Figure S6) and were retrieved by dispersing them into fresh water. The yield of the product under continuous flow was estimated to be about 42 and 83 μg per minute of samples exiting the VFD (outside) and adhering to the inside of the VFD tube (inside), respectively. The IONPs were recovered by placing a magnet next to the wall of the vial containing the colloidal solution. Characterization using XRD on 0.1 mL/min sample (both inside and outside) confirmed the presence of magnetite (Figure 4d) with an average particle size of around 12 nm (Figure 4e1), with no evidence for the presence of other materials, including carbon.

High-resolution transmission electron microscopy (HRTEM) and SAED showed that IONPs both exiting the tube under flow and retained inside the tube are single crystals and showed two shapes of spheres and hexagonal prisms (Figure 5).[8] Magnetite nanohexagons are usually obtained using chemical synthesis from iron acetylacetonate under high temperatures of up to 290 °C for extended time. However, the average particle size for such hexagons is about 85 nm or up to a 100 nm,[32,34] whereas in our case, they are between 15 and 20 nm (Figure 5b). The generation of hexagonal particles at smaller and narrow size range using laser ablation further highlights the significance of our findings and the versatility of the VFD.

Both samples exhibit superparamagnetic characteristics with the highest saturation magnetization (M_s) value of about 41 A m^2 kg^{-1} at room temperature (Figure 6a,b),[6] which is consistent with the average particle size of about 12 nm in

both samples. The slight decrease in M_s for the sample (retained) can be attributed to the slightly disordered surface and reduced crystallinity,[12,28] which could be because of the longer exposure to the laser beam. The low-field interval of both magnetization curves reveals the negligibility of the hysteresis which again implies the superparamagnetism.[35] Apart from generating single-phase crystals, laser-ablated IONPs prepared using the VFD have higher saturation magnetization than those prepared using conventional laser ablation processing in water. For example, the M_s of IONPs prepared by Vahabzadeh et al.[2] in water was 14.8−22.5 emu/g with H_c of 11.5−22 Oe, which was not considered as superparamagnetic. Maneeratanasarn et al.[36] reported the generation of amorphous α-Fe$_2$O$_3$ nanoparticles with a low saturation magnetization of only 1.315 emu/g using laser ablation in water. The superparamagnetic IONPs prepared using the VFD resulted from precise control of the oxidative states, particle size, and morphology during the process.

The plasma plume that is a mixture of atoms, ions, and radicals is generated in air and reacts immediately,[37] with particles colliding with each other[12] and then with uptake in the dynamic thin film in the VFD. In the presence of a gas or liquid phase in a conventional sense, diffusion-driven nucleation and aggregation processes play an important role in the generation and size control of the particles.[2] However, this is not readily adjustable. Experiments conducted without any liquid in the VFD showed a significantly larger particle size of about 20.7 nm compared to 14.2 nm when formed in the presence of water (Table S1). To decouple the effect of oxygen, the reaction was conducted under N$_2$ gas (Figure S7), but this resulted in negligible formation of iron oxide. Thus, the presence of oxygen is essential for the reaction. Liu et al.[38] reported that the rapid quenching of species generated at high temperature using laser ablation generates pure iron oxide species. In this context, the rapid heat dissipation from the VFD may be important in determining the nature of the iron oxide species generated during the processing.

■ CONCLUSIONS

In summary, a novel highly selective method has been developed for preparing single-phase superparamagnetic magnetite nanoparticles directly by laser ablation of a metal iron in the presence of both gas and liquid phases. The

nanoparticles obtained under different conditions showed spherical or hexagonal shapes, with relative uniform average diameters of around 15 nm. Compared with conventional processes, this method can selectively control phase composition and the size and shape of the particles in establishing a new application for VFD. Future experiments will investigate the fabrication of protective coatings on the particle surface to stabilize the structure and further improve the magnetism.

■ EXPERIMENTAL SECTION

The experiments were carried out under both the confined mode and continuous flow mode of operation of the VFD, as indicated in Figure 1. In a typical confined mode experiment, 15 min processing time was carried out in a rapidly rotating tube at θ 45° tilt with a simultaneously 5 ns pulsed laser at 1064 nm (pulsed Q-switch Nd:YAG laser) with an 8 mm diameter laser beam irradiating a high purity (>99.998%) iron rod 5 mm in diameter, which was immobilized on a stainless steel jet feed (Figure 1a). In a continuous flow, experiments were conducted under the same condition, as described in the confine mode, except that stainless steel jet feeds were used for both immobilizing the iron rod and delivering liquid into the rapidly rotating tube (Figure 1b). Optimizing the flow rate of water involved studying 0.1, 0.5, and 1.0 mL/min flow rates, using a syringe pump. Under both processing conditions, the laser beam was positioned perpendicular to the target surface, with the formation of hot and high-pressure plasma plumes containing iron atoms and ions expanding in all directions (Figure 1c,d). The laser beam was focused about 7.5 mm away from the thin film surface with the expanding plumes restrained within the VFD tube.

As prepared samples were dried in the open air as per previous studies[2] and were characterized by UV−vis spectrophotometer (Varian Cary 50) in the 200−1000 nm range in a quartz cell and X-ray diffraction (Bruker D8 ADVANCE ECO, Co-Kα, λ = 1.79 Å) with radiation generated at 35 kV and 28 mA and a grazing incidence angle (3°) in the 2θ range of 20°−80°. The lattice parameter calculations were obtained using the EVA software. The average crystallite size was estimated using Debye−Scherrer equation. Particle sizes/morphology and crystalline structures were observed using dynamic light scattering (Malvern Instrument, UK), scanning electron microscopy, TEM, and AFM. TEM was conducted on an FEI TECNAI F20 microscope operated at 200 kV. Raman spectroscopy was performed with an excitation wavelength of 532 nm for an integration time of 30 s to differentiate the presence of magnetite and maghemite. As processed materials were investigated using Raman spectroscopy after drop-casting, one drop of the colloidal material on a glass substrate. Magnetic measurements were carried out using a Quantum Design PPMS with ACMS option at room temperature (295 K) by saturating the sample in a field of up to 15 000 Oe.

■ ASSOCIATED CONTENT

ⓢ Supporting Information

The Supporting Information is available free of charge on the ACS Publications website at DOI: 10.1021/acsomega.8b01606.

　　Additional characterization data including Raman, UV−vis, FT-IR, and XRD (PDF)

■ AUTHOR INFORMATION

Corresponding Authors
*E-mail: colin.raston@flinders.edu.au. Phone: +61 8 82017958. Fax: +61 8 8201290 (C.R.).
*E-mail: wei.zhang@flinders.edu.au. Phone: +61 8 72218557. Fax: +61 8 72218555 (W.Z.).

ORCID
Xuan Luo: 0000-0002-8811-3143
Jin Zou: 0000-0001-9435-8043
Colin L. Raston: 0000-0003-4753-0079

Notes
The authors declare no competing financial interest.

■ REFERENCES

(1) Demirer, G. S.; Okur, A. C.; Kizilel, S. Synthesis and Design of Biologically Inspired Biocompatible Iron Oxide Nanoparticles for Biomedical Applications. *J. Mater. Chem. B* **2015**, *3*, 7831−7849.

(2) Vahabzadeh, E.; Torkamany, M. J. Iron Oxide Nanocrystals Synthesis by Laser Ablation in Water: Effect of Laser Wavelength. *J. Cluster Sci.* **2014**, *25*, 959−968.

(3) Majewski, P.; Thierry, B. Functionalized Magnetite Nanoparticles-Synthesis, Properties, and Bio-Applications. *Crit. Rev. Solid State Mater. Sci.* **2007**, *32*, 203−215.

(4) Liu, B.; Wang, D.; Huang, W.; Yao, A.; Kamitakahara, M.; Ioku, K. Preparation of Magnetite Nanoparticles Coated with Silica via a Sol-gel Approach. *J. Ceram. Soc. Jpn.* **2007**, *115*, 877−881.

(5) Chin, A. B.; Yaacob, I. I. Synthesis and Characterization of Magnetic Iron Oxide Nanoparticles via w/o Microemulsion and Massart's Procedure. *J. Mater. Process. Technol.* **2007**, *191*, 235−237.

(6) Thorek, D. L. J.; Chen, A. K.; Czupryna, J.; Tsourkas, A. Superparamagnetic Iron Oxide Nanoparticle Probes for Molecular Imaging. *Ann. Biomed. Eng.* **2006**, *34*, 23−38.

(7) Li, S.-Z.; Hong, Y. C.; Uhm, H. S.; Li, Z.-K. Synthesis of Nanocrystalline Iron Oxide Particles by Microwave Plasma Jet at Atmospheric Pressure. *Jpn. J. Appl. Phys.* **2004**, *43*, 7714−7717.

(8) Amendola, V.; Riello, P.; Meneghetti, M. Magnetic Nanoparticles of Iron Carbide, Iron Oxide, Iron@Iron Oxide, and Metal Iron Synthesized by Laser Ablation in Organic Solvents. *J. Phys. Chem. C* **2011**, *115*, 5140−5146.

(9) Dadashi, S.; Poursalehi, R.; Delavari, H. Structural and Optical Properties of Pure Iron and Iron Oxide Nanoparticles Prepared via Pulsed Nd:YAG Laser Ablation in Liquid. *Procedia Mater. Sci.* **2015**, *11*, 722−726.

(10) Barcikowski, S.; Hahn, A.; Kabashin, A. V.; Chichkov, B. N. Properties of Nanoparticles Generated during Femtosecond Laser Machining in Air and Water. *Appl. Phys. A* **2007**, *87*, 47−55.

(11) Franzel, L.; Bertino, M. F.; Huba, Z. J.; Carpenter, E. E. Synthesis of Magnetic Nanoparticles by Pulsed Laser Ablation. *Appl. Surf. Sci.* **2012**, *261*, 332−336.

(12) Maneeratanasarn, P.; Van Khai, T.; Kim, S. Y.; Choi, B. G.; Shim, K. B. Synthesis of Phase-controlled Iron Oxide Nanoparticles by Pulsed Laser Ablation in Different Liquid Media. *Phys. Status Solidi* **2013**, *210*, 563−569.

(13) Dudoitis, V.; Ulevičius, V.; Račiukaitis, G.; Špirkauskaitė, N.; Plauškaitė, K. Generation of Metal Nanoparticles by Laser Ablation. *Lith. J. Phys.* **2011**, *51*, 248−259.

(14) Hahn, A.; Barcikowski, S.; Chichkov, B. Influences on Nanoparticle Production during Pulsed Laser Ablation. *J. Laser Micro/Nanoeng.* **2008**, *3*, 73−77.

(15) Britton, J.; Stubbs, K. A.; Weiss, G. A.; Raston, C. L. Vortex Fluidic Chemical Transformations. *Chem.—Eur. J.* **2017**, *23*, 13270−13278.

(16) Alharbi, T. M. D.; Harvey, D.; Alsulami, I. K.; Dehbari, N.; Duan, X.; Lamb, R. N.; Lawrance, W. D.; Raston, C. L. Shear Stress Mediated Scrolling of Graphene Oxide. *Carbon* **2018**, *137*, 419−424.

(17) Vimalanathan, K.; Gascooke, J. R.; Suarez-Martinez, I.; Marks, N. A.; Kumari, H.; Garvey, C. J.; Atwood, J. L.; Lawrance, W. D.; Raston, C. L. Fluid Dynamic Lateral Slicing of High Tensile Strength Carbon Nanotubes. *Sci. Rep.* **2016**, *6*, 22865.

(18) Vimalanathan, K.; Chen, X.; Raston, C. L. Shear Induced Fabrication of Intertwined Single Walled Carbon Nanotube Rings. *Chem. Commun.* **2014**, *50*, 11295−11298.

(19) Yasmin, L.; Chen, X.; Stubbs, K. A.; Raston, C. L. Optimising a Vortex Fluidic Device for Controlling Chemical Reactivity and Selectivity. *Sci. Rep.* **2013**, *3*, 2282.

(20) Luo, X.; Smith, P.; Raston, C. L.; Zhang, W. Vortex Fluidic Device-Intensified Aqueous Two Phase Extraction of C-Phycocyanin from Spirulina maxima. *ACS Sustainable Chem. Eng.* **2016**, *4*, 3905−3911.

(21) Britton, J.; Meneghini, L. M.; Raston, C. L.; Weiss, G. A. Accelerating Enzymatic Catalysis Using Vortex Fluidics. *Angew. Chem., Int. Ed.* **2016**, *55*, 11387−11391.

(22) Yuan, T. Z.; Ormonde, C. F. G.; Kudlacek, S. T.; Kunche, S.; Smith, J. N.; Brown, W. A.; Pugliese, K. M.; Olsen, T. J.; Iftikhar, M.; Raston, C. L.; Weiss, G. A. Shear-Stress-Mediated Refolding of Proteins from Aggregates and Inclusion Bodies. *ChemBioChem* **2015**, *16*, 393−396.

(23) D'Alonzo, N. J.; Eggers, P. K.; Raston, C. L. Vortex Fluidics Synthesis of Polymer Coated Superparamagnetic Magnetite Nanoparticles. *New J. Chem.* **2017**, *41*, 552−558.

(24) Ji, Y. Ions removal by iron nanoparticles: a study on solid-water interface with zeta potential. *Colloids Surf., A* **2014**, *444*, 1−8.

(25) Fazio, E.; Santoro, M.; Lentini, G.; Franco, D.; Guglielmino, S. P. P.; Neri, F. Iron Oxide Nanoparticles Prepared by Laser Ablation: Synthesis, Structural Properties and Antimicrobial Activity. *Colloids Surf., A* **2016**, *490*, 98−103.

(26) Kumar, P. A.; Ray, S.; Chakraverty, S.; Sarma, D. D. Magnetoresistance and electroresistance effects in Fe3O4 nanoparticle system. *J. Exp. Nanosci.* **2014**, *9*, 391−397.

(27) Bersani, D.; Lottici, P. P.; Montenero, A. Micro-Raman investigation of iron oxide films and powders produced by sol-gel syntheses. *J. Raman Spectrosc.* **1999**, *30*, 355−360.

(28) Chourpa, I.; Douziech-Eyrolles, L.; Ngaboni-Okassa, L.; Fouquenet, J.-F.; Cohen-Jonathan, S.; Soucé, M.; Marchais, H.; Dubois, P. Molecular Composition of Iron Oxide Nanoparticles, Precursors for Magnetic Drug Targeting, as Characterized by Confocal Raman Microspectroscopy. *Analyst* **2005**, *130*, 1395−1403.

(29) Lee, Y.-J. The Second Order Raman Spectroscopy in Carbon Crystallinity. *J. Nucl. Mater.* **2004**, *325*, 174−179.

(30) Marton, M.; Vojs, M.; Zdravecká, E.; Himmerlich, M.; Haensel, T.; Krischok, S.; Kotlár, M.; Michniak, P.; Veselý, M.; Redhammer, R. Raman Spectroscopy of Amorphous Carbon Prepared by Pulsed Arc Discharge in Various Gas Mixtures. *J. Spectrosc.* **2013**, *2013*, 1.

(31) Amendola, V.; Riello, P.; Polizzi, S.; Fiameni, S.; Innocenti, C.; Sangregorio, C.; Meneghetti, M. Magnetic iron oxide nanoparticles with tunable size and free surface obtained via a "green" approach based on laser irradiation in water. *J. Mater. Chem.* **2011**, *21*, 18665−18673.

(32) Shebanova, O. N.; Lazor, P. Raman study of magnetite (Fe3O4): laser-induced thermal effects and oxidation. *J. Raman Spectrosc.* **2003**, *34*, 845−852.

(33) Eom, Y.; Abbas, M.; Noh, H.; Kim, C. Morphology-controlled synthesis of highly crystalline Fe3O4 and CoFe2O4 nanoparticles using a facile thermal decomposition method. *RSC Adv.* **2016**, *6*, 15861−15867.

(34) Wang, H.; Shrestha, T. B.; Basel, M. T.; Pyle, M.; Toledo, Y.; Konecny, A.; Thapa, P.; Ikenberry, M.; Hohn, K. L.; Chikan, V.; Troyer, D. L.; Bossmann, S. H. Hexagonal Magnetite Nanoprisms: Preparation, Characterization and Cellular Uptake. *J. Mater. Chem. B* **2015**, *3*, 4647−4653.

(35) Jafari, A.; Salouti, M.; Shayesteh, S. F.; Heidari, Z.; Rajabi, A. B.; Boustani, K.; Nahardani, A. Synthesis and Characterization of Bombesin-superparamagnetic Iron Oxide Nanoparticles as a Targeted Contrast Agent for Imaging of Breast Cancer using MRI. *Nanotechnology* **2015**, *26*, 075101.

(36) Maneeratanasarn, P.; Van Khai, T.; Kim, S. Y.; Choi, B. G.; Shim, K. B. Synthesis of Phase-controlled Iron Oxide Nanoparticles by Pulsed Laser Ablation in Different Liquid Media. *Phys. Status Solidi A* **2013**, *210*, 563−569.

(37) Salik, M.; Hanif, M.; Wang, J.; Zhang, X. Plasma Properties of Nano-second Laser Ablated Iron Target in Air. *Int. J. Phys. Sci.* **2013**, *8*, 1738−1745.

(38) Liu, P.; Cai, W.; Zeng, H. Fabrication and Size-Dependent Optical Properties of FeO Nanoparticles Induced by Laser Ablation in a Liquid Medium. *J. Phys. Chem. C* **2008**, *112*, 3261−3266.